materials

MDPI

Article

Chemical Stability of Ti_3C_2 MXene with Al in the Temperature Range 500–700 °C

Jing Zhang, Shibo Li *, Shujun Hu and Yang Zhou

Centre of Materials Science and Engineering, School of Mechanical and Electronic Control Engineering, Beijing Jiaotong University, Beijing 100044, China; 16121356@bjtu.edu.cn (J.Z.); 16116341@bjtu.edu.cn (S.H.); yzhou@bjtu.edu.cn (Y.Z.)

* Correspondence: shbli1@bjtu.edu.cn; Tel.: +86-10-51685554

Received: 21 September 2018; Accepted: 12 October 2018; Published: 15 October 2018

Abstract: $Ti_3C_2T_x$ MXene, a new 2D nanosheet material, is expected to be an attractive reinforcement of metal matrix composites because its surfaces are terminated with Ti and/or functional groups of –OH, –O, and –F which improve its wettability with metals. Thus, new $Ti_3C_2T_x$/Al composites with strong interfaces and novel properties are desired. To prepare such composites, the chemical stability of $Ti_3C_2T_x$ with Al at high temperatures should be investigated. This work first reports on the chemical stability of $Ti_3C_2T_x$ MXene with Al in the temperature range 500–700 °C. $Ti_3C_2T_x$ is thermally stable with Al at temperatures below 700 °C, but it reacts with Al to form Al_3Ti and TiC at temperatures above 700 °C. The chemical stability and microstructure of the $Ti_3C_2T_x$/Al samples were investigated by differential scanning calorimeter, X-ray diffraction analysis, scanning electron microscopy, and transmission electron microscopy.

Keywords: $Ti_3C_2T_x$; MXene; aluminum; chemical stability; microstructure

1. Introduction

MXenes, as a new family of two-dimensional (2D) materials, have attracted much attention because of their unusual combination of mechanical, physical, and chemical properties [1–10]. The MXenes are produced by the selective extraction of A-element from the layered MAX phases (where M is an early transition metal, A is an A group element, and X is C or N), such as Ti_3AlC_2, Ti_2AlC, and Ti_3SiC_2 by either HF solutions [1,2,11–13], HCl/fluoride salt solutions [3,14–18], or HF/oxidant solutions [19]. After removal of the A layers from MAX, the top and bottom surfaces of the bare MXene monolayer or single sheet are terminated by the redistribution of M atoms with metallic bonds. Hence, the MXenes exhibit metallic conductivity. However, the exposed M surfaces of MXenes are always attached by functional groups such as hydroxyl (–OH), oxide (–O), or fluorine (–F) after etching in acid solutions. Hence, the general formula $M_{n+1}X_nT_x$ (where T_x denotes the MXene terminal groups and x is number of terminal groups, n = 1, 2, or 3) is always used to represent the MXenes.

MXenes have similar structure and properties to graphene and other 2D nanosheets. The attractive 2D MXenes are now being used in a wide range of applications in energy storage, electromagnetic interference shielding, water purification, gas- and biosensors, lubrication, photo-, electro- and chemical catalysis, and as reinforcement for composites [3,5–7,12,20–30].

In the 2D MXene group, $Ti_3C_2T_x$ is the first reported and the most explored material because it is easily synthesized from the Ti_3AlC_2 precursor using HF solution [1]. The 2D $Ti_3C_2T_x$ single nanosheet is micrometers in width but less than a nanometer in thickness. Hence, the $Ti_3C_2T_x$ MXene, with its attractive properties and high aspect ratios, has already been used as a reinforcement in composites. So far, the majority of the current work on composites containing $Ti_3C_2T_x$ has focused on polymer

matrix composites [30–34], but less attention has been devoted to the use of $Ti_3C_2T_x$ to reinforce metal matrix composites.

In recent years, there has been intense research into Al matrix composites reinforced with 1D carbon nanotubes (CNTs) and 2D graphene to improve their mechanical properties [35–38]. However, there remains a challenge to overcome weak interfaces in the CNT/Al and graphene/Al composites, due to the poor wettability of CNTs and graphene with Al matrix.

Using $Ti_3C_2T_x$ to reinforce the Al metal matrix composites possibly endows the $Ti_3C_2T_x$/Al composites with a strong interfacial strength because the surfaces of $Ti_3C_2T_x$ nanosheets are terminated with Ti or functional groups such as –OH, –O, and –F. It has been reported that the surface modification of CNTs by –O and –OH functional groups enhanced the interfacial bonding between metals and CNTs [39,40]. The functionalized 2D nanotubes can be employed as reinforcing fillers [41,42]. In addition, the –F and –O surface functional groups on the $Ti_3C_2T_x$ nanosheets can be eliminated at high temperatures [43,44]. The loss of surface functional groups possibly promotes the bonding of Ti surface atoms on bare Ti_3C_2 with Al. However, work on the $Ti_3C_2T_x$/Al composites has been much less focused so far. The ability to practically produce $Ti_3C_2T_x$/Al composites remains to be demonstrated. Al matrix composites reinforced with 1D CNTs and 2D graphene have always been prepared in the temperature range 500–640 °C. To practically prepare $Ti_3C_2T_x$/Al composites and to understand the chemical stability of $Ti_3C_2T_x$ with Al, the temperature range 500–700 °C was selected in the present study.

The purpose of this work was to assess the chemical stability of $Ti_3C_2T_x$ with Al in the temperature range from 500 °C to 700 °C by X-ray diffraction, differential scanning calorimetry, scanning electron microscopy, and transmission electron microscopy methods. The interfaces between $Ti_3C_2T_x$ and Al were characterized.

2. Materials and Methods

$Ti_3C_2T_x$ MXene was prepared by acid etching of Ti_3AlC_2 powder. The fabrication of Ti_3AlC_2 has been described elsewhere [45]. Briefly, Ti (325-mesh, >99.2% purity), Al (particle size <5 μm, 99.5% purity), and C (graphite, <45 μm, >99.5% purity) powders with a molar ratio of Ti:Al:C = 3:1.1:2 were mixed for 10 h. The mixed mixture was cold-pressed to form compacts with a diameter of 50 mm and a height of approximately 5 mm. The compacts were pressurelessly sintered at 1450 °C for 1 h in an Ar atmosphere. The sintered samples were pulverized and then sifted with a 300-mesh sieve to make Ti_3AlC_2 powder. A total of 2.5 g of Ti_3AlC_2 powder was immersed in 60 mL of 40% HF solution in a polytetrafluoroethylene (PTFE) container. A heating magnetic stirrer was used to continuously stir the solution in the PTFE container at 50 °C for 0.5 h. The solution was centrifugally separated in a centrifuge (LD-4, Jinan Wohong Experimental instrument Co., Ltd., Jinan, China) with a rotation rate of 4000 rpm for 5 min and then washed with deionized water until a pH of about 7 was attained. The obtained sediment was vacuum dried at 80 °C for 24 h to make the desired $Ti_3C_2T_x$ powder. The prepared $Ti_3C_2T_x$ powder was sieved with a 200-mesh sieve.

Al and 10 wt % $Ti_3C_2T_x$ powders were mixed in a polypropylene container with agate balls for 10 h in a rotary drum type ball-miller with a speed of 150 rpm. The mixture was cold-pressed in a stainless steel mold with 100 MPa to form pellets with a diameter of 20 mm and a height of about 5 mm. The pellets were put into a graphite crucible coated with boron nitride and then sintered in the absence of additional pressure conditions in the temperature range 500–700 °C for 1 h in Ar.

The phase composition of the samples before and after sintering was identified by X-ray diffraction (XRD) analysis using a D/Max 2200 PC diffractometer (Rigaku Co. Ltd., Tokyo, Japan) applying monochromatic Cu Kα radiation. The operating voltage and current were 40 kV and 20 mA, respectively. The microstructures of the sintered samples were characterized with a ZEISS EVO 18 scanning electron microscope (SEM) equipped with an energy-dispersive spectrometer system (EDS), and a JEM-2100F (JEOL Ltd., Tokyo, Japan) transmission electron microscope (TEM) with an operating voltage of 200 kV. TEM images were processed with the software RADIUS Desktop 2.0

(EMSIS GmbH, Muenster, Germany). Differential scanning calorimetry (DSC) analysis was used to measure the amount of energy absorbed or released by the $Ti_3C_2T_x$/Al mixture heated in a NETZSCH STA 449F3 thermal analyzer (Netzsch, Germany) from room temperature to 800 °C with a heating rate of 15 °C/min in flowing Ar.

3. Results and Discussion

The DSC curve of the $Ti_3C_2T_x$/Al mixture, together with that of pure Al for comparison, is presented in Figure 1. A broad endothermic peak appearing at around 110 °C on the DSC curve for $Ti_3C_2T_x$/Al is ascribed to the evaporation of water absorbed in the interlayers of $Ti_3C_2T_x$. The thermal gravity (TG) curve correspondingly exhibits a downward trend on mass loss. A sharp endothermic peak at 664 °C corresponds to the melting of Al (660 °C). Comparing the two DSC curves, it can be found that there is an exothermic peak at 717 °C on the DSC curve of $Ti_3C_2T_x$/Al, which can be ascribed to the occurrence of a reaction between $Ti_3C_2T_x$ and Al. In the temperature range from 150 °C to 700 °C, the TG curve reveals a gradual mass loss, possibly due to the removal of surface groups such as –OH and –O. Zhou et al. [43] reported that there was a broad and weak exothermic peak in the DSC curve for the pure $Ti_3C_2T_x$ in the temperature range 200–800 °C in Ar due to the loss of surface groups. Shah et al. [46] reported that the bonding energies for –O, –OH, and –F groups in the $Ti_3C_2T_x$ MXene are 530.3 eV, 531.3 eV, and 685.1 eV, respectively. The bonding energies suggest that the removal sequence of the surface groups is –O > –OH > –F. Li and coworkers [44] reported that the disappearance of –OH and –O groups occurred at approximately 500 K and the removal of –F group was required at a high temperature of 1173 K in Ar. Sang and coworkers also confirmed that the functional group of –O was removed after annealing of $Ti_3C_2T_x$ MXene at 500 °C [47].

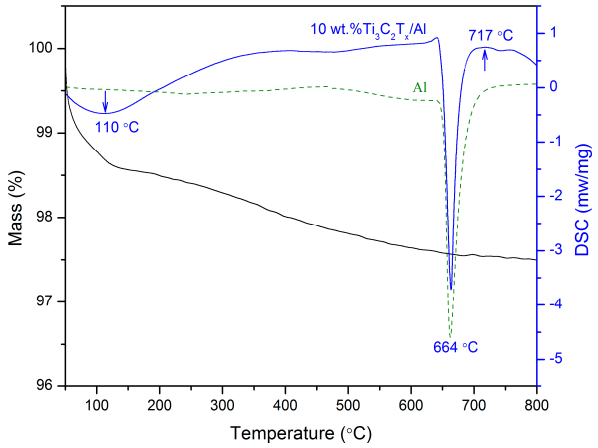

Figure 1. DSC analysis for 10 wt % Ti_3C_2/Al mixture in the temperature range 50–800 °C, together with Al for comparison.

To identify the reaction products and to characterize the microstructure, the samples sintered at temperatures from 500 °C to 700 °C were examined using XRD, SEM, and TEM.

Figure 2 shows XRD patterns of 10 wt % $Ti_3C_2T_x$/Al samples before and after sintering at various temperatures. Before sintering, only $Ti_3C_2T_x$ MXene and Al are detected, see Figure 2a. The broad peaks indicate the nanosheet structure of $Ti_3C_2T_x$. After sintering at 650 °C, some sharp diffraction peaks but with lower intensities appeared, in addition to the peaks corresponding to Al. These peaks are in good agreement with the simulated peaks for pure Ti_3C_2 and $Ti_3C_2F_2$, see Figure 2b. It should be noted that the (002) peak at 8.7°, (004) peak at 17.98°, and (006) peak at 27.38° belonging to the $Ti_3C_2T_x$ MXene disappeared in the XRD patterns of the sintered samples, see Figure 2b,c. The XRD results suggest that water molecules associated with the interlayer functional groups such as –O and –OH were gradually removed from 100 °C to 650 °C. The loss of water and functional groups causes a decrease in the basal space distance, or, alternatively, the newly formed surfaces possibly bond to form

a new structure, which potentially induces the disappearance of basal peaks. The disappearance of basal plane peaks is similar to those for some layered compounds such as montmorillonite [48] and tetratitanate [49]. However, the diffractogram of the sample sintered at 700 °C shows the appearance of new phases of Al_3Ti and TiC, indicating the occurrence of a reaction between $Ti_3C_2T_x$ and Al at 700 °C. This result is in good agreement with the DSC analysis. Some weak peaks belonging to unreacted Ti_3C_2 and $Ti_3C_2F_2$ can still be found. However, several peaks appearing in Figure 2c were not confirmed.

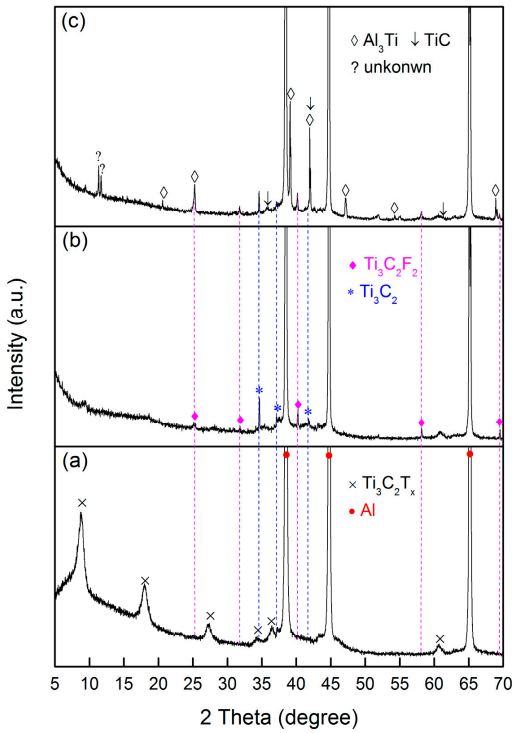

Figure 2. XRD patterns of the Ti_3C_2/Al mixture before (**a**), and after heat treatment at (**b**) 650 °C and (**c**) 700 °C in Ar for 1 h.

Figure 3 presents the morphologies of the raw Al and $Ti_3C_2T_x$ powders and microstructures of the sintered samples. The raw Al particles are spherical, and each $Ti_3C_2T_x$ particle has stacked multilayers, as shown in Figure 3a. After sintering at 650 °C, the polished surface shows that the $Ti_3C_2T_x$ particles mainly distribute at the Al grain boundaries, see Figure 3b. No other new phases were detected in the sample sintered at 650 °C. The fracture surface clearly shows the stacked multilayers of $Ti_3C_2T_x$ particles, see Figure 3c.

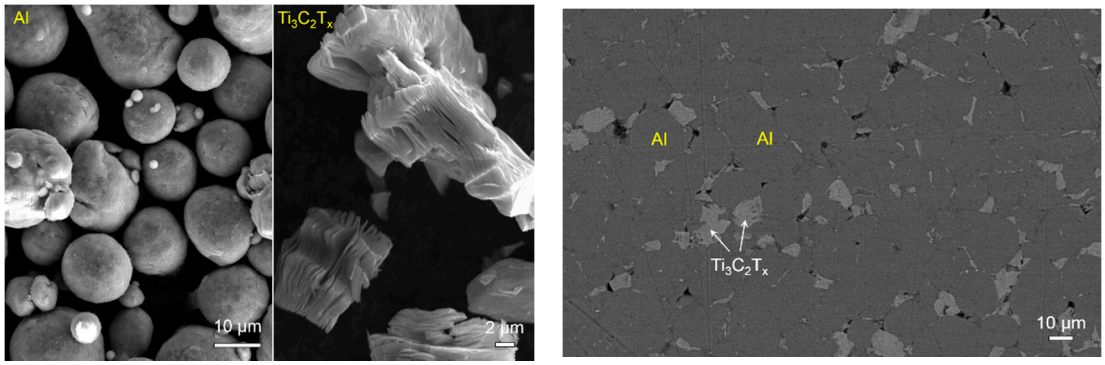

(**a**) (**b**)

Figure 3. *Cont.*

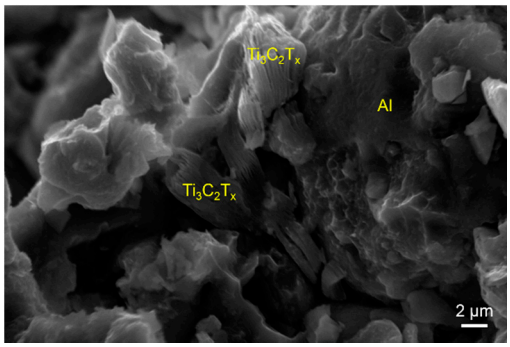

(**c**)

Figure 3. SEM micrographs of the initial powders (**a**), and polished surface (**b**) and fracture surface (**c**) of the samples sintered at 650 °C in Ar for 1 h. The left- and right-hand side micrographs in (**a**) show the morphologies of Al and $Ti_3C_2T_x$ powders, respectively.

Figure 4a presents a TEM image of a multilayer $Ti_3C_2T_x$ flake. The EDS line analysis, see Figure 4b, reveals the Al signal in the $Ti_3C_2T_x$ flake, indicating the diffusion of Al atoms into the multilayers of $Ti_3C_2T_x$. The interlayer spacing areas of $Ti_3C_2T_x$ provide active sites for Al nucleation and crystal growth. It should be noted that the F element was detected in the $Ti_3C_2T_x$ multilayers, but O was mainly distributed in the areas between the $Ti_3C_2T_x$ flake and Al grains. The presence of F in the multilayers suggests that the surface-layer termination of MXene is mostly F, i.e., $Ti_3C_2F_2$. The –O group in $Ti_3C_2T_x$ may react with Al to form Al_2O_3.

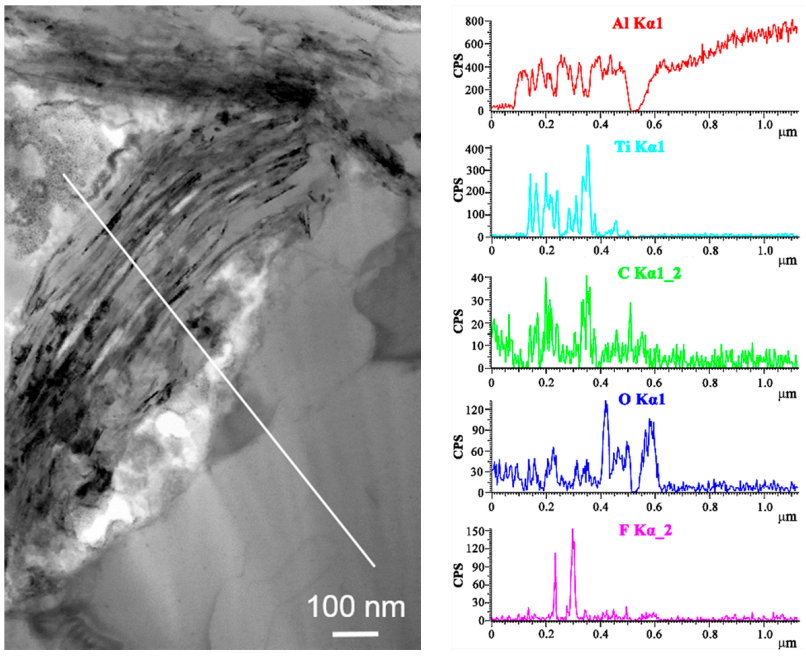

(**a**) (**b**)

Figure 4. TEM image (**a**) and EDS results of the $Ti_3C_2T_x$/Al sample sintered at 650 °C (**b**). The EDS scan analysis along the line in (**a**) showing the elemental distribution of Al, Ti, C, O, and F.

Figure 5 presents the TEM micrographs of a $Ti_3C_2T_x$/Al sample sintered at 650 °C. These $Ti_3C_2T_x$ flakes are from several nanometers to tens of nanometers in thickness, indicating the thinner flake is composed of at least two $Ti_3C_2T_x$ layers, see Figure 5a. The interspaces in the $Ti_3C_2T_x$ flakes are filled with Al. A high-resolution TEM (HRTEM) image shows that the interlayer spacing of $Ti_3C_2T_x$ is about 0.855 nm, see Figure 5b. This value is smaller than the value of 1.17 to 1.28 nm for the initial $Ti_3C_2T_x$ flakes due to the removal of functional groups after heat treatment at 650 °C. The HRTEM image of the

Ti_3C_2/Al interface reveals that the lattices of the Ti_3C_2 and Al regions are in direct contact, as shown in Figure 5c. The interface is clean and continuous. Neither precipitates nor amorphous regions are observed at the interface. The above observation suggests that the Ti_3C_2/Al interface is chemically and structurally stable at 650 °C.

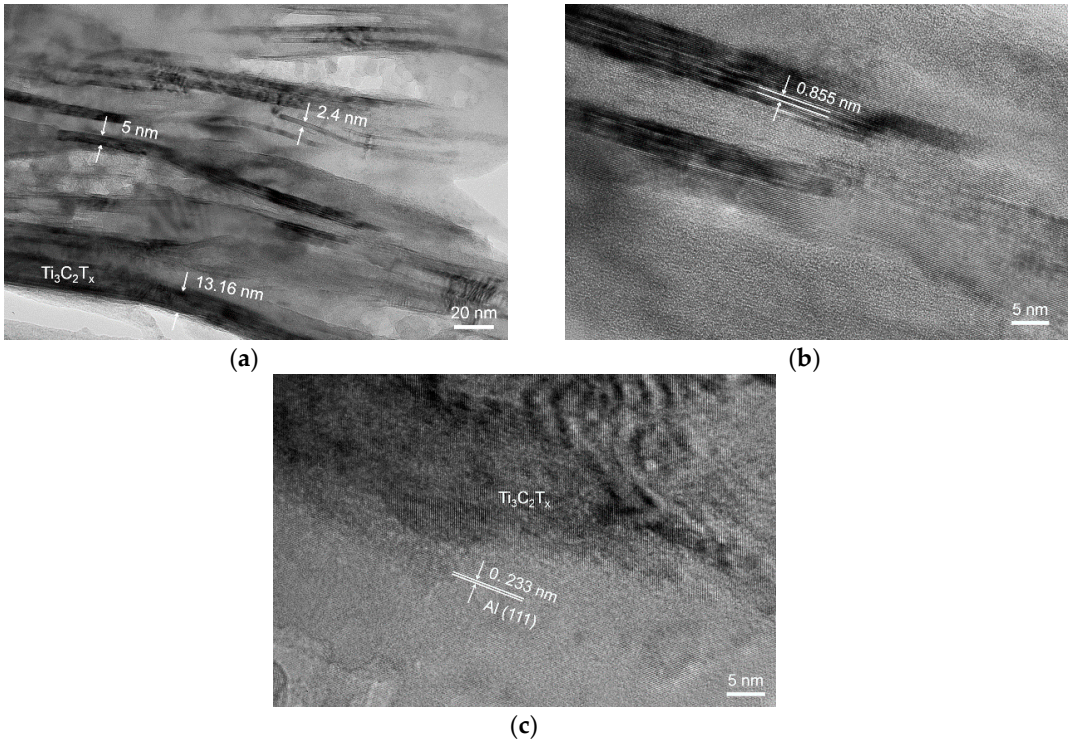

Figure 5. TEM images of the sample sintered at 650 °C. (**a**) A TEM micrograph showing stacked multilayers of $Ti_3C_2T_x$, (**b**) a high-resolution TEM (HRTEM) micrograph of $Ti_3C_2T_x$, and (**c**) a HRTEM micrograph of $Ti_3C_2T_x$/Al interface.

4. Conclusions

The chemical stability of Ti_3C_2 with Al was investigated in the temperature range 500–700 °C in Ar for 1 h. $Ti_3C_2T_x$ is thermally stable with Al at 650 °C, but it reacts with Al to form Al_3Ti and TiC at 700 °C. For the $Ti_3C_2T_x$/Al sample sintered at 650 °C, the $Ti_3C_2T_x$/Al interface is clean and continuous, without precipitates and amorphous regions. The loss of water molecules and the removal of functional groups of –OH and –O induces a decrease in the interlayer spacing of $Ti_3C_2T_x$. The present work demonstrates the possibility to prepare Ti_3C_2Tx MXene reinforced Al or other metal matrix composites under certain processing conditions.

Author Contributions: Conceptualization, S.L. and Y.Z.; methodology, S.L.; formal analysis, J.Z. and S.H.; investigation, J.Z. and S.H.; writing—original draft preparation, J.Z.; writing—review and editing, S.L.; supervision, S.L.; project administration, S.L.; funding acquisition, S.L.

Funding: This work was funded by the National Natural Science Foundation of China, grant number 51772020, Beijing Natural Science Foundation, grant number 2182058, and Beijing Government Funds for the Constructive Project of Central Universities.

Conflicts of Interest: The authors declare no conflict of interest.

References

1. Naguib, M.; Kurtoglu, M.; Presser, V.; Lu, J.; Niu, J.; Heon, M.; Hultman, L.; Gogotsi, Y.; Barsoum, M.W. Two-dimensional nanocrystals produced by exfoliation of Ti_3AlC_2. *Adv. Mater.* **2011**, *23*, 4248–4253. [CrossRef] [PubMed]

2. Mashtalir, O.; Naguib, M.; Mochalin, V.N.; Dall'Agnese, Y.; Heon, M.; Barsoum, M.W.; Gogotsi, Y. Intercalation and delamination of layered carbides and carbonitrides. *Nat. Commun.* **2013**, *4*, 1716. [CrossRef] [PubMed]
3. Ghidiu, M.; Lukatskaya, M.R.; Zhao, M.Q.; Gogotsi, Y.; Barsoum, M.W. Conductive two-dimensional titanium carbide 'Clay' with high volumetric capacitance. *Nature* **2014**, *516*, 78–81. [CrossRef] [PubMed]
4. Naguib, M.; Mochalin, V.N.; Barsoum, M.W.; Gogotsi, Y. MXenes: A new family of two-dimensional materials. *Adv. Mater.* **2014**, *26*, 992–1005. [CrossRef] [PubMed]
5. Sun, S.; Liao, C.; Hafez, A.M.; Zhu, H.; Wu, S. Two-dimensional MXenes for energy storage. *Chem. Eng. J.* **2018**, *338*, 27–45. [CrossRef]
6. Sun, Y.; Chen, D.; Liang, Z. Two-dimensional MXenes for energy storage and conversion applications. *Mater. Today Energy* **2017**, *5*, 22–36. [CrossRef]
7. Ran, J.; Gao, G.; Li, F.T.; Ma, T.Y.; Du, A.; Qiao, S.Z. Ti_3C_2 MXene co-catalyst on metal sulfide photo-absorbers for enhanced visible-light photocatalytic hydrogen production. *Nat. Commun.* **2017**, *8*, 13907. [CrossRef] [PubMed]
8. Ng, V.M.H.; Huang, H.; Zhou, K.; Lee, P.S.; Que, W.; Xu, J.Z.; Kong, L.B. Recent progress in layered transition metal carbides and/or nitrides (MXenes) and their composites: Synthesis and applications. *J. Mater. Chem. A* **2017**, *5*, 3039–3068.
9. Ling, Z.; Ren, C.E.; Zhao, M.Q.; Yang, J.; Giammarco, J.M.; Qiu, J.; Barsoum, M.W.; Gogotsi, Y. Flexible and conductive MXene films and nanocomposites with high capacitance. *Proc. Natl. Acad. Sci. USA* **2014**, *111*, 16676–16681. [CrossRef] [PubMed]
10. Miranda, A.; Halim, J.; Barsoum, M.W.; Lorke, A. Electronic properties of freestanding $Ti_3C_2T_x$ MXene monolayers. *Appl. Phys. Lett.* **2016**, *108*, 033102. [CrossRef]
11. Anasori, B.; Xie, Y.; Beidaghi, M.; Lu, J.; Hosler, B.C.; Hultman, L.; Kent, P.R.; Gogotsi, Y.; Barsoum, M.W. Two-dimensional ordered, double transition metals carbides (MXenes). *ACS Nano* **2015**, *9*, 9507–9516. [CrossRef] [PubMed]
12. Naguib, M.; Halim, J.; Lu, J.; Cook, K.M.; Hultman, L.; Gogotsi, Y.; Barsoum, M.W. New two-dimensional niobium and vanadium carbides as promising materials for Li-Ion batteries. *J. Am. Chem. Soc.* **2013**, *135*, 15966–15969. [CrossRef] [PubMed]
13. Ghidiu, M.; Naguib, M.; Shi, C.; Mashtalir, O.; Pan, L.M.; Zhang, B.; Yang, J.; Gogotsi, Y.; Billinge, S.J.; Barsoum, M.W. Synthesis and characterization of two-dimensional Nb_4C_3 (MXene). *Chem. Commun.* **2014**, *50*, 9517–9520. [CrossRef] [PubMed]
14. Halim, J.; Kota, S.; Lukatskaya, M.R.; Naguib, M.; Zhao, M.Q.; Moon, E.J.; Pitock, J.; Nanda, J.; May, S.J.; Gogotsi, Y.; et al. Synthesis and characterization of 2D molybdenum carbide (MXene). *Adv. Funct. Mater.* **2016**, *26*, 3118–3127. [CrossRef]
15. Liu, F.; Zhou, A.; Chen, J.; Jia, J.; Zhou, W.; Wang, L.; Hu, Q. Preparation of Ti_3C_2 and Ti_2C MXenes by fluoride salts etching and methane adsorptive properties. *Appl. Surf. Sci.* **2017**, *416*, 781–789. [CrossRef]
16. Zhang, T.; Pan, L.; Tang, H.; Du, F.; Guo, Y.; Qiu, T.; Yang, J. Synthesis of two-dimensional $Ti_3C_2T_x$ MXene using HCl+LiF etchant: Enhanced exfoliation and delamination. *J. Alloy. Compd.* **2017**, *695*, 818–826. [CrossRef]
17. Naguib, M.; Unocic, R.R.; Armstrong, B.L.; Nanda, J. Large-scale delamination of multi-layers transition metal carbides and carbonitrides 'MXenes'. *Dalton Trans.* **2015**, *44*, 9353–9358. [CrossRef] [PubMed]
18. Halim, J.; Lukatskaya, M.R.; Cook, K.M.; Lu, J.; Smith, C.R.; May, S.J.; Hultman, L.; Gogotsi, Y.; Eklund, P.; Barsoum, M.W. Transparent conductive two-dimensional titanium carbide epitaxial thin films. *Chem. Mater.* **2014**, *26*, 2374–2381. [CrossRef] [PubMed]
19. Alhabeb, M.; Maleski, K.; Mathis, T.S.; Sarycheva, A.; Hatter, C.B.; Uzun, S.; Levitt, A.; Gogotsi, Y. Selective etching of silicon from Ti_3SiC_2 (MAX) produces 2D titanium carbide (MXene). *Angew. Chem.* **2018**. [CrossRef]
20. Han, M.; Yin, X.; Wu, H.; Hou, Z.; Song, C.; Li, X.; Zhang, L.; Cheng, L. Ti_3C_2 MXenes with modified surface for high-performance electromagnetic absorption and shielding in the X-Band. *ACS Appl. Mater. Interfaces* **2016**, *8*, 21011–21019. [CrossRef] [PubMed]
21. Shahzad, F.; Alhabeb, M.; Hatter, C.B.; Anasori, B.; Hong, S.M.; Koo, C.M.; Gogotsi, Y. Electromagnetic interference shielding with 2D transition metal carbides (MXenes). *Science* **2016**, *353*, 1137–1140. [CrossRef] [PubMed]

22. Zhang, Q.; Teng, J.; Zou, G.; Peng, Q.; Du, Q.; Jiao, T.; Xiang, J. Efficient phosphate sequestration for water purification by unique sandwich-like MXene/Magnetic iron oxide nanocomposites. *Nanoscale* **2016**, *8*, 7085–7093. [CrossRef] [PubMed]
23. Chen, J.; Chen, K.; Tong, D.; Huang, Y.; Zhang, J.; Xue, J.; Huang, Q.; Chen, T. CO_2 and temperature dual responsive "Smart" MXene phases. *Chem. Commun.* **2015**, *51*, 314–317. [CrossRef] [PubMed]
24. Xiao, B.; Li, Y.C.; Yu, X.F.; Cheng, J. MXenes: Reusable materials for NH_3 sensor or capturer by controlling the charge injection. *Sens. Actuators B* **2016**, *235*, 103–109. [CrossRef]
25. Xu, B.; Zhu, M.; Zhang, W.; Zhen, X.; Pei, Z.; Xue, Q.; Zhi, C.; Shi, P. Ultrathin MXene-micropattern-based field-effect transistor for probing neural activity. *Adv. Mater.* **2016**, *28*, 3333–3339. [CrossRef] [PubMed]
26. Yang, J.; Chen, B.; Song, H.; Tang, H.; Li, C. Synthesis, characterization, and tribological properties of two-dimensional Ti_3C_2. *Cryst. Res. Technol.* **2014**, *49*, 926–932. [CrossRef]
27. Zhang, X.; Xue, M.; Yang, X.; Wang, Z.; Luo, G.; Huang, Z.; Sui, X.; Li, C. Preparation and tribological properties of $Ti_3C_2(OH)_2$ nanosheets as additives in base oil. *RSC Adv.* **2015**, *5*, 2762–2767. [CrossRef]
28. Ma, T.Y.; Cao, J.L.; Jaroniec, M.; Qiao, S.Z. Interacting carbon nitride and titanium carbide nanosheets for high-performance oxygen evolution. *Angew. Chem. Int. Ed.* **2015**, *55*, 1138–1142. [CrossRef] [PubMed]
29. Peng, C.; Yang, X.; Li, Y.; Yu, H.; Wang, H.; Peng, F. Hybrids of two-dimensional Ti_3C_2 and TiO_2 exposing {001} facets toward enhanced photocatalytic activity. *ACS Appl. Mater. Interfaces* **2016**, *8*, 6051–6060. [CrossRef] [PubMed]
30. Boota, M.; Anasori, B.; Voigt, C.; Zhao, M.Q.; Barsoum, M.W.; Gogotsi, Y. Pseudocapacitive electrodes produced by oxidant–Free polymerization of pyrrole between the layers of 2D titanium carbide (MXene). *Adv. Mater.* **2016**, *28*, 1517–1522. [CrossRef] [PubMed]
31. Ye, Q.; Chen, T. Exploring the potential of exfoliated ternary ultrathin Ti_4AlN_3 nanosheets for fabricating hybrid patterned polymer brushes. *RSC Adv.* **2015**, *5*, 70339–70344. [CrossRef]
32. Zhang, H.; Wang, L.; Chen, Q.; Li, P.; Zhou, A.; Cao, X.; Hu, Q. Preparation, Mechanical and antifriction performance of MXene/polymer composites. *Mater. Des.* **2016**, *92*, 682–689. [CrossRef]
33. Liu, Y.H.; Zhang, J.K.; Zhang, X.; Li, Y.F.; Wang, J.T. $Ti_3C_2T_x$ filler effect on the proton conduction property of polymer electrolyte membrane. *ACS Appl. Mater. Interfaces* **2016**, *8*, 20352–20363. [CrossRef] [PubMed]
34. Cao, Y.; Deng, Q.; Liu, Z.; Shen, D.; Wang, T.; Huang, Q.; Du, S.; Jiang, N.; Lin, C.T.; Yu, J. Enhanced thermal properties of poly (vinylidenefluoride) composites with ultrathin nanosheets of MXene. *RSC Adv.* **2017**, *7*, 20494–20501. [CrossRef]
35. Kuzumaki, T.; Miyazawa, K.; Ichinose, H.; Ito, K. Processing of carbon nanotube reinforced aluminum composite. *J. Mater. Res.* **1998**, *13*, 2445–2449. [CrossRef]
36. He, C.; Zhao, N.; Shi, C.; Du, X.; Li, J.; Li, H.; Cui, Q. An approach to obtaining homogeneously dispersed carbon nanotubes in Al powders for preparing reinforced Al-Matrix composites. *Adv. Mater.* **2007**, *19*, 1128–1132. [CrossRef]
37. Tjong, S.C. Recent progress in the development and properties of novel metal matrix nanocomposites reinforced with carbon nanotubes and graphene nanosheets. *Mater. Sci. Eng. R* **2013**, *74*, 281–350. [CrossRef]
38. Li, Z.; Guo, Q.; Li, Z.; Fan, G.; Xiong, D.B.; Su, Y.; Zhang, J.; Zhang, D. Enhanced mechanical properties of graphene (reduced graphene oxide)/aluminum composites with a bioinspired nanolaminated structure. *Nano Lett.* **2015**, *15*, 8077–8083. [CrossRef] [PubMed]
39. Park, M.; Kim, B.H.; Kim, S.; Han, D.S.; Kim, G.; Lee, K.R. Improved binding between copper and carbon nanotubes in a composite using oxygen-containing functional groups. *Carbon* **2011**, *49*, 811–818. [CrossRef]
40. Lee, H.J.; Choi, W.S.; Nguyen, T.; Lee, Y.B.; Lee, H. An easy method for direct metal coordination reaction on unoxidized single-walled carbon nanotubes. *Carbon* **2011**, *49*, 5150–5157. [CrossRef]
41. Cavallaro, G.; Danilushkina, A.A.; Evtugyn, V.G.; Lazzara, G.; Milioto, S.; Parisi, F.; Rozhima, E.V.; Fakhrullin, R.F. Halloysite nanotubes: Controlled access and release by smart gates. *Nanomaterials* **2017**, *7*, 199. [CrossRef] [PubMed]
42. Lazzara, G.; Cavallaro, G.; Panchal, A.; Fakhrullin, R.; Stavitskaya, A.; Vinokurov, V.; Lvov, Y. An assembly of organic-inorganic composites using halloysite clay nanotubes. *Curr. Opin. Colloid Interface Sci.* **2018**, *35*, 42–50. [CrossRef]
43. Li, Z.; Wang, L.; Sun, D.; Zhang, Y.; Liu, B.; Hu, Q.; Zhou, A. Synthesis and thermal stability of two-dimensional carbide MXene Ti_3C_2. *Mater. Sci. Eng. B* **2015**, *191*, 33–40. [CrossRef]

44. Li, J.; Du, Y.; Huo, C.; Wang, S.; Cui, C. Thermal stability of two-dimensional Ti_2C nanosheets. *Ceram. Int.* **2015**, *41*, 2631–2635. [CrossRef]
45. Hu, S.; Li, S.B.; Li, H.; Zhou, Y. Large-scale growth of TiB_2 hexagonal sheets. *J. Alloy. Compd.* **2017**, *690*, 930–935. [CrossRef]
46. Shah, S.A.; Habib, T.; Gao, H.; Gao, P.; Sun, W.; Green, M.J.; Radovic, M. Template–Free 3D titanium carbide ($Ti_3C_2T_x$) MXene particles crumpled by capillary forces. *Chem. Commun.* **2017**, *53*, 400–403. [CrossRef] [PubMed]
47. Sang, X.; Xie, Y.; Yilmaz, D.E.; Lotfi, R.; Alhabeb, M.; Ostadhossein, A.; Anasori, B.; Sun, W.; Li, X.; Xiao, K.; et al. In situ atomistic insight into the growth mechanisms of single layer 2D transition metal carbides. *Nat. Comm.* **2018**, *9*, 2266:1–2266:9. [CrossRef] [PubMed]
48. Yang, J.; Ding, J. Preparation and characterization of alumina-pillared ultrafine layered tetratitanate. *Mater. Lett.* **2004**, *58*, 3872–3875. [CrossRef]
49. Kooli, F.; Liu, Y.; Alshahattet, S.F.; Messali, M.; Bergaya, F. Reaction of acid activated montmorillonites with hexadecyl trimethylammonium bromide solution. *Appl. Clay Sci.* **2009**, *43*, 357–363. [CrossRef]